

Three-Dimensional Data Compression and Fast High-Quality Reconstruction for Phased Array Weather Radar

Ryosuke Kawami*	Student Member,	Daichi Kitahara*	Non-member
Akira Hirabayashi ^{*a)}	Non-member,	Eiichi Yoshikawa**	Non-member
Hiroshi Kikuchi ^{***}	Member,	Tomoo Ushio ^{****}	Senior Member

(Manuscript received April 11, 2019, revised Aug. 16, 2019)

This paper proposes a fast high-quality three-dimensional (3D) compressed sensing for a phased array weather radar (PAWR), which is capable of spatially and temporally high-resolution observation of the atmosphere. Because of the high-resolution, the PAWR generates huge observation data of approximately 500 megabytes every thirty seconds. To transfer this huge data in a public internet line for real time weather forecast, an efficient data compression technology is required. The proposed method compresses the PAWR data by randomly transferring several measurements only in the troposphere, and then reconstructs the missing measurements for each small 3D tensor data by minimizing a cost function based on a prior knowledge on weather phenomena. The minimizer of the cost function can be quickly computed by using a convex optimization algorithm with Nesterov's acceleration technique. Numerical simulations using real PAWR data show the effectiveness of the proposed method compared to conventional two-dimensional methods.

Keywords: Phased array weather radar, data compression, compressed sensing, convex optimization, Nesterov's acceleration

1. Introduction

Occurrence of extreme weather events is getting more frequent⁽¹⁾. Among such events, there exist thunderstorms with heavy rain caused by quick growth of cumulonimbus clouds. Thunderstorms only take tens of minutes from their generation to decay, while classical weather radars equipped with a parabolic antenna take five or ten minutes for sparse scan of the whole sky. Thus the temporal and spatial resolution is not sufficient for observation of these thunderstorms.

A phased array weather radar (PAWR)⁽²⁾⁻⁽⁴⁾ was developed in order to overcome the above limitation. That developed in Osaka University achieved the temporal resolution of thirty seconds for scanning a hemisphere of a radius sixty kilometers. Furthermore, the spatial resolution along the range axis was improved to one hundred meters, which means that the number of sampling points in the range axis increased to 600. Those in the azimuth and the elevation axes increased to 300 and 110, respectively. The measurements include thirteen as-

pects of weather phenomena, and two bytes are used to describe each aspect. As a result, huge data of 490.9 megabytes is generated every thirty seconds, and a data transfer without any compression technique needs a transfer rate of 130.9 megabits per second (Mbps). Thus the current PAWR system exploits a private internet line with some cost, but it makes real time weather forecast on the network difficult.

To transfer the PAWR data in a public internet line, an efficient compression technique is necessary as well as a high-quality reconstruction algorithm. A standard public internet line of 100 Mbps at most can only maintain 30 to 40 Mbps in average. By assuming that 35 Mbps is available, the required compression rate becomes 26.73% approximately. Thus we set 25% compression rate as our goal in this paper.

To this end, we exploit random selection for compression scheme as used in several existing papers⁽⁵⁾⁻⁽⁹⁾. In the PAWR system, the observed data is processed as shown in the left column of Fig. 1. The observed data are mixtures of the backscattered signals from various elevation angles within the antenna beamwidth. A digital beamforming technique⁽¹⁰⁾⁻⁽¹²⁾ divides the mixed signals into the backscattered signals of the individual elevations. Then, the demixed signals are used to compute thirteen weather parameters including the reflection intensity, whose data size is 37.8 megabytes for one rotation of the PAWR. The computational cost to obtain each parameter is not ignorable. In a scenario without compression, the entire 37.8 megabytes data are transferred to a remote server and then analyzed. On the other hand, we exploit random selection after the beamforming as shown in the right column of Fig. 1. Then, we can reduce not only the data size of the reflection intensity to 9.44 megabytes but also the cost for its computation. Since the entire reflection intensity data are not

a) Correspondence to: Akira Hirabayashi. E-mail: akirahr@media.ritsumeikai.ac.jp

* Graduate School of Information Science and Engineering, Ritsumeikan University
1-1-1 Noji-higashi, Kusatsu, Shiga 525-8577, Japan

** Aeronautical Technology Directorate, Japan Aerospace Exploration Agency
6-13-1 Osawa, Mitaka, Tokyo 181-0015, Japan

*** Center for Space Science and Radio Engineering, The University of Electro-Communications
1-5-1 Chofugaoka, Chofu, Tokyo 182-8585, Japan

**** Division of Electrical, Electronic and Infocommunications Engineering, Osaka University
2-1 Yamadaoka, Suita, Osaka 565-0871, Japan

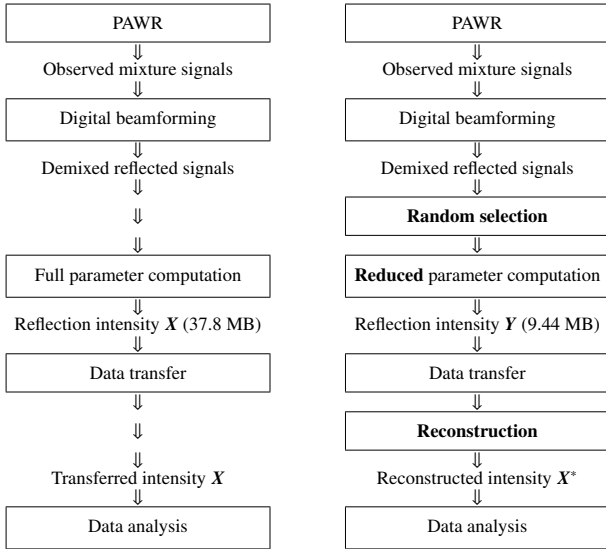


Fig. 1. Flowcharts of original and our data processing.

computed, we cannot exploit a Huffman code, even though it can theoretically achieve the lowest compression rate.

The random selection compression scheme matches with reconstruction techniques in compressed sensing (CS) ^{(13)–(15)}. CS was first applied to radars for point targets ^{(16)–(18)} and then applied to weather radars ^{(5)–(9)(19)(20)}. For example, Mishra *et al.* used a low-rank matrix approximation to reconstruct two-dimensional (2D) slices, in the entire three-dimensional (3D) PAWR data, from compressed slices ⁽⁵⁾. Shimamura *et al.* proposed a one-dimensional (1D) reconstruction algorithm that promotes the sparsity in a wavelet domain ⁽⁶⁾. In our previous work, we proposed a two-dimensional (2D) reconstruction algorithm which promotes the local similarity and the sparsity of 2D slice data in the spatial and the frequency domains, respectively ⁽⁷⁾⁽⁸⁾. In this method, matrices are extracted as *slice data for fixed elevations*, in the same manner as the method of Mishra *et al.* Such matrices are generated only after each thirty seconds rotation of the PAWR. Hence the PAWR system has to transfer these matrices while saving new measurements in the next rotation. As a result, our previous technique is not efficient with respect to memory usage although the reconstruction quality is better than the other methods ⁽⁵⁾⁽⁶⁾.

In this paper, not only to reduce the memory usage but also to further improve the reconstruction quality, we propose a 3D reconstruction method. The PAWR sequentially captures *2D slice data for fixed azimuth directions*, and then creates the entire 3D PAWR data by combining all 2D slice data. If we apply our previous 2D reconstruction method ⁽⁷⁾⁽⁸⁾ to such a slice in each azimuth direction, we can transfer the PAWR data with low memory usage because we do not need to wait the thirty seconds rotation. However, the reconstruction quality of this simple strategy is not good because the local similarity along the elevation axis is lower than that along the azimuth axis. To achieve both of low memory usage and high reconstruction accuracy, we have proposed a 3D reconstruction method ⁽⁹⁾, and this paper proposes its improved version. In the 3D reconstruction method ⁽⁹⁾, we combine several contiguous slices into a 3D tensor and compress it. We randomly select and transfer some measurements of the 3D tensor only in the troposphere. Then, we reconstruct the 3D tensor from

the compressed tensor by minimizing a convex cost function based on the following prior knowledge on the PAWR data. First, all measurements outside of the troposphere are zeros because there is no weather events. Second, the reconstructed data should be consistent with the compressed one. Third, the 3D total variation is relatively small because of the local similarity in the spatial domain. Fourth, the ℓ_1 -norm of the 3D discrete cosine transform (DCT) coefficients is also small because of the sparsity in the frequency domain. Since the cost function is convex, the minimizer can be efficiently found by using one of the convex optimization techniques ^{(21)–(23)}.

In the previous paper ⁽⁹⁾, we further improved the convergence speed by Nesterov’s acceleration technique ^{(24)–(27)}, but one issue that the cost function is *not strongly convex*[†] was not considered. For a strongly convex cost function, the convergence speed of the alternating direction method of multipliers (ADMM) can be improved by applying Nesterov’s acceleration to dual variables ⁽²⁶⁾. However, since the proposed cost function is not strongly convex, the previous algorithm ⁽⁹⁾ cannot guarantee the convergence to the optimal solution. Although Nesterov’s acceleration with a restart rule is proposed to theoretically guarantee the convergence ⁽²⁶⁾, this strategy is slow because it takes much time, in every iteration, to judge whether the restart should be done or not. Instead, in this paper, we apply the acceleration technique only in the first several iterations, and after that the standard ADMM iterations are used. Numerical simulations using real PAWR data show that the proposed method outperforms the conventional 2D reconstruction algorithms ⁽⁵⁾⁽⁷⁾⁽⁸⁾ with less computational time.

The rest of this paper is organized as follows. Section 2 formulates our PAWR data compression scheme. In Section 3.1, we define a cost function for 3D reconstruction and propose a blockwise reconstruction algorithm based on a convex optimization technique. Section 3.2 describes Nesterov’s acceleration for the reconstruction algorithm. Section 4 shows the effectiveness of the proposed algorithm by numerical simulations using real data. Finally, Section 5 concludes this paper.

2. Data Compression by Random Selection

In this paper, we focus on the reflection intensity among thirteen weather parameters observed by the PAWR ^{(2)–(4)}. The other parameters can be handled in similar ways. The reflection intensities are observed as a 3D tensor $\mathbf{X} \in \mathbb{R}^{N_R \times N_A \times N_E}$, and we denote by $x[n_R, n_A, n_E] \in \mathbb{R}$ the (n_R, n_A, n_E) -entry of \mathbf{X} , where $1 \leq n_R \leq N_R := 600$, $1 \leq n_A \leq N_A := 300$, and $1 \leq n_E \leq N_E := 110$, i.e., the number of measurements is $N := N_R N_A N_E = 19,800,000$.

The PAWR can observe the reflection intensities within a hemisphere of a radius sixty kilometers. This hemisphere includes the out of the troposphere and $x[n_R, n_A, n_E]$ is 0 there. We use this knowledge for both sampling and reconstruction. Let H_{tro} be the height of the troposphere, where the curvature of the earth is not taken into account. In order to compress the original data \mathbf{X} , we randomly select $M (< N)$ measurements within regions in which the height is lower than H_{tro} and then convert $(N - M)$ unselected measurements into 0. This compression process is denoted by $\mathcal{A} : \mathbb{R}^{N_R \times N_A \times N_E} \rightarrow \mathbb{R}^{N_R \times N_A \times N_E}$,

[†] A function $f : \mathbb{R}^N \rightarrow \mathbb{R} \cup \{\infty\}$ is called *convex* if $f(\lambda \mathbf{x} + (1 - \lambda)\mathbf{y}) \leq \lambda f(\mathbf{x}) + (1 - \lambda)f(\mathbf{y})$ for all $\mathbf{x}, \mathbf{y} \in \mathbb{R}^N$ and all $\lambda \in (0, 1)$, and *strongly convex* if $f(\lambda \mathbf{x} + (1 - \lambda)\mathbf{y}) < \lambda f(\mathbf{x}) + (1 - \lambda)f(\mathbf{y})$ for all $\mathbf{x}, \mathbf{y} \in \mathbb{R}^N$ and all $\lambda \in (0, 1)$.

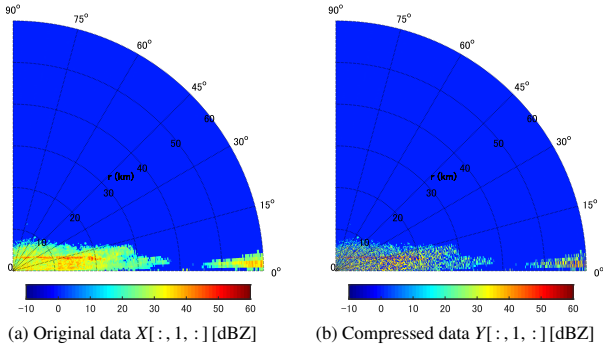


Fig. 2. Original data and compressed data.

the compressed data is expressed as $Y := \mathcal{A}(X)$, and the compression ratio is defined by $\alpha := M/N \in (0, 1)$.

An example of a pair of the original observed data X and the compressed data Y is shown in Fig. 2, where slices of the 1st azimuth direction are extracted from the entire 3D tensors. The original data X was acquired on March 30th, 2014, by the PAWR equipped in Suita Campus of Osaka University, Japan, and the compressed data Y retains only 25% measurements among X . Now, we must recover the missing measurements from the selected remaining ones and their positions. The next section proposes a high-quality reconstruction method.

3. Three-Dimensional Reconstruction Algorithm Based on Blockwise Convex Optimization

The proposed method in this paper is an improved version of our previous 3D reconstruction method⁽⁹⁾. In Section 3.1, we summarize our previous method⁽⁹⁾, where the data fidelity term is modified from the cost into constraint. In Section 3.2, we apply Nesterov's acceleration while considering the non-strong convexity which was ignored in the previous paper⁽⁹⁾.

3.1 Proposed 3D Blockwise Reconstruction In the PAWR system, a 2D matrix data $X[:, n_A, :] \in \mathbb{R}^{N_R \times N_E}$ as in Fig. 2(a) is acquired at the same time. By rotationally acquiring $X[:, n_A, :]$ ($n_A = 1, 2, \dots, N_A$) in sequence and combining them, the entire 3D tensor data $X \in \mathbb{R}^{N_R \times N_A \times N_E}$ is generated. In this section, we propose to divide the entire tensor X into small tensors and to reconstruct each tensor in sequence.

At first, with some factor s of N_A , we divide the original data X and the compressed one Y into N_A/s tensors $X_l := (X[:, (l-1)s+1, :], X[:, (l-1)s+2, :], \dots, X[:, ls, :]) \in \mathbb{R}^{N_R \times s \times N_E}$ and $Y_l = \mathcal{A}_l(X_l) \in \mathbb{R}^{N_R \times s \times N_E}$ ($l = 1, 2, \dots, N_A/s$). We suppose that each compression process $\mathcal{A}_l : \mathbb{R}^{N_R \times s \times N_E} \rightarrow \mathbb{R}^{N_R \times s \times N_E}$ has the same compression ratio M/N , i.e., we randomly select sM/N_A measurements from each X_l within regions in which the height is lower than H_{tro} .

To reconstruct the complete measurements X_l from the randomly selected ones Y_l , we exploit four characteristics of X_l . First, the measurements outside of the troposphere are 0 as mentioned before. Let us denote the set of all $X_l \in \mathbb{R}^{N_R \times s \times N_E}$ satisfying this condition by \mathcal{S} . Second, the observation of X_l should be consistent with Y_l . Third, the reflection intensities are locally similar because rain falling areas exist continuously. Fourth, we suppose that X_l can be sparsely described in the frequency domain. On the basis of the above characteristics, we reconstruct X as $X^* := (X_1^*, X_2^*, \dots, X_{N_A/s}^*) \in \mathbb{R}^{N_R \times N_A \times N_E}$, where each block X_l^* ($l = 1, 2, \dots, N_A/s$) is re-

constructed by solving a convex optimization problem

$$X_l^* := \underset{X_l \in \mathcal{S} \text{ s.t. } \mathcal{A}_l(X_l) = Y_l}{\text{argmin}} \quad \text{TV}(X_l) + \lambda \|C(X_l)\|_1. \quad \dots \dots (1)$$

In (1), $\lambda > 0$, $C : \mathbb{R}^{N_R \times s \times N_E} \rightarrow \mathbb{R}^{N_R \times s \times N_E}$ denotes the 3D DCT, $\|X_l\|_1 := \sum_{n_R=1}^{N_R} \sum_{n_A=1}^s \sum_{n_E=1}^{N_E} |x_l[n_R, n_A, n_E]|$, and the total variation is defined by

$$\begin{aligned} \text{TV}(X_l) := & \sum_{n_R=1}^{N_R-1} \sum_{n_A=1}^s \sum_{n_E=1}^{N_E} |x_l[n_R+1, n_A, n_E] - x_l[n_R, n_A, n_E]| \\ & + \sum_{n_R=1}^{N_R} \sum_{n_A=1}^{s-1} \sum_{n_E=1}^{N_E} |x_l[n_R, n_A+1, n_E] - x_l[n_R, n_A, n_E]| \\ & + \sum_{n_R=1}^{N_R} \sum_{n_A=1}^s \sum_{n_E=1}^{N_E-1} |x_l[n_R, n_A, n_E+1] - x_l[n_R, n_A, n_E]|. \end{aligned}$$

In (1), the cost function is convex and two constraint sets are also convex[†]. Therefore, this problem is a convex optimization problem and can be solved by the simultaneous direction method of multipliers (SDMM)⁽²²⁾, which is a special case of ADMM⁽²¹⁾, as follows.

Let $x_l := \text{vec}(X_l) \in \mathbb{R}^{\widehat{N}}$ ($\widehat{N} := sN_RN_E$) be a vectorized version of a 3D tensor $X_l \in \mathbb{R}^{N_R \times s \times N_E}$, and the inverse mapping of vec is denoted by ten , i.e., $X_l = \text{ten}(x_l)$. Let $A_l \in \mathbb{R}^{\widehat{N} \times \widehat{N}}$ be a diagonal matrix which converts the unselected measurements of x_l into 0 while retaining the selected ones. Define

$$D_{N_R} := \begin{pmatrix} -1 & 1 & 0 & \dots & 0 \\ 0 & -1 & 1 & \dots & 0 \\ \vdots & \ddots & \ddots & \ddots & \vdots \\ 0 & \dots & 0 & -1 & 1 \end{pmatrix} \in \mathbb{R}^{(N_R-1) \times N_R},$$

and also define $D_s \in \mathbb{R}^{(s-1) \times s}$ and $D_{N_E} \in \mathbb{R}^{(N_E-1) \times N_E}$ in the same manner. The identity matrix and the 1D DCT matrix of size $K \times K$ are denoted by I_K and C_K , respectively. By defining matrices, with the use of the Kronecker product \otimes , as

$$\begin{cases} L_1 := I_{N_E} \otimes I_s \otimes I_{N_R}, & L_2 := I_{N_E} \otimes I_s \otimes D_{N_R}, \\ L_3 := I_{N_E} \otimes D_s \otimes I_{N_R}, & L_4 := D_{N_E} \otimes I_s \otimes I_{N_R}, \\ L_5 := C_{N_E} \otimes C_s \otimes C_{N_R}, & L_6 := I_{N_E} \otimes I_s \otimes I_{N_R}, \end{cases}$$

and defining $g_1(\mathbf{y}_1) := 0$ if $A_l \mathbf{y}_1 = \text{vec}(Y_l)$, $g_1(\mathbf{y}_1) := \infty$ if $A_l \mathbf{y}_1 \neq \text{vec}(Y_l)$, $g_i(\mathbf{y}_i) := \|\mathbf{y}_i\|_1$ ($i = 2, 3, 4$), $g_5(\mathbf{y}_5) := \lambda \|\mathbf{y}_5\|_1$, $g_6(\mathbf{y}_6) := 0$ if $\text{ten}(\mathbf{y}_6) \in \mathcal{S}$, and $g_6(\mathbf{y}_6) := \infty$ if $\text{ten}(\mathbf{y}_6) \notin \mathcal{S}$, a vectorized version of X_l^* in (1) is expressed as

$$x_l^* = \underset{x_l \in \mathbb{R}^{\widehat{N}}}{\text{argmin}} \sum_{i=1}^6 g_i(L_i x_l). \quad \dots \dots (2)$$

The vector x_l^* in (2) can be computed by SDMM as shown in Algorithm 1, and the original tensor data is reconstructed by $X_l^* = \text{ten}(x_l^*)$. In Algorithm 1, $Q := \sum_{i=1}^6 L_i^T L_i \in \mathbb{R}^{\widehat{N} \times \widehat{N}}$ is invertible and the analytic form of Q^{-1} can be derived in a similar way as in our previous method⁽⁷⁾⁽⁸⁾ without any product of huge matrices of size $\widehat{N} \times \widehat{N}$. Moreover, for any $\gamma > 0$, each proximity operator $\text{prox}_{\gamma g_i}(\mathbf{w}_i) := \underset{\mathbf{y}_i}{\text{argmin}} g_i(\mathbf{y}_i) + \frac{1}{2\gamma} \|\mathbf{y}_i - \mathbf{w}_i\|_2^2$ ($i = 1, 2, \dots, 6$) can be easily computed⁽²²⁾⁽²³⁾.

[†] Since the range resolution of the PAWR is 100 [m] and the elevation resolution is $\frac{\pi}{220}$ [rad], the height corresponding to $x_l[n_R, n_A, n_E]$ is given by $100 n_R \sin(\frac{n_E \pi}{220})$ [m]. Furthermore, the height of the troposphere H_{tro} [m] is fixed, and hence \mathcal{S} is expressed as $\mathcal{S} := \{X_l \in \mathbb{R}^{N_R \times s \times N_E} \mid x_l[n_R, n_A, n_E] = 0 \text{ for all } (n_R, n_A, n_E) \text{ s.t. } 100 n_R \sin(\frac{n_E \pi}{220}) > H_{\text{tro}}\}$. This set is clearly convex.

Algorithm 1 3D PAWR data reconstruction

Input: $Y_l \in \mathbb{R}^{N_R \times s \times N_E}$, $\gamma \in (0, \infty)$, and an integer I_{\max}

- 1: $\mathbf{y}_{i,0} \leftarrow L_i \text{vec}(Y_l)$ and $\mathbf{z}_{i,0} \leftarrow \mathbf{0}$ ($i = 1, 2, \dots, 6$)
- 2: **for** $k = 1, 2, \dots, I_{\max}$ **do**
- 3: $\mathbf{x}_k \leftarrow Q^{-1} \sum_{i=1}^6 L_i^T (\mathbf{y}_{i,k-1} - \mathbf{z}_{i,k-1})$
- 4: $\mathbf{y}_{i,k} \leftarrow \text{prox}_{\gamma g_i}(L_i \mathbf{x}_k + \mathbf{z}_{i,k-1})$ ($i = 1, 2, \dots, 6$)
- 5: $\mathbf{z}_{i,k} \leftarrow \mathbf{z}_{i,k-1} + L_i \mathbf{x}_k - \mathbf{y}_{i,k}$ ($i = 1, 2, \dots, 6$)
- 6: **end for**

Output: $\mathbf{x}_l^* \leftarrow \mathbf{x}_k$

3.2 Nesterov's Acceleration for Algorithm 1 In this section, we improve the convergence speed of Algorithm 1 by Nesterov's acceleration technique^{(24)–(27)}. Goldstein *et al.* proposed Fast ADMM as an accelerated variant of ADMM, and the convergence rate can be improved from $O(1/k)$ to $O(1/k^2)$ for a strongly convex optimization problem⁽²⁶⁾. Fortunately, SDMM is just a special case of ADMM, and hence we apply Nesterov's technique to dual variables following the paper⁽²⁶⁾.

Since the function in (2) is not strongly convex, we should use Fast ADMM with a restart rule for stable computations (see Algorithm 8 in the paper⁽²⁶⁾). However, in our case, this strategy cannot accelerate Algorithm 1 because it takes much time, in every iteration, to judge whether the restart should be done or not. Through our numerical experiments, we found that the restart hardly happens in the first several iterations, e.g., five iterations for the problem in (2). Therefore, we apply Nesterov's technique only in the first P iterations without checking the restart condition, and after that the same iterations as in Algorithm 1 are continued. Algorithm 2 summarizes this idea, where we use different parameters γ_1 and γ_2 for computing prox_{γ_i} to achieve the best convergence speed.

Note that Algorithms 1 and 2 are suitable for parallel computing. Hence, GPU implementations of these algorithms, in which the computation for each block X_l is assigned to each core, would further accelerate the reconstruction process.

Algorithm 2 Fast 3D PAWR data reconstruction

Input: $Y_l \in \mathbb{R}^{N_R \times s \times N_E}$, $\gamma_1, \gamma_2 \in (0, \infty)$, and integers $P < I_{\max}$

- 1: $\mathbf{y}_{i,0} \leftarrow L_i \text{vec}(Y_l)$ and $\mathbf{z}_{i,0} \leftarrow \mathbf{0}$ ($i = 1, 2, \dots, 6$)
- 2: $\mathbf{y}_{i,\frac{1}{2}} \leftarrow \mathbf{y}_{i,0}$ and $\mathbf{z}_{i,\frac{1}{2}} \leftarrow \mathbf{z}_{i,0}$ ($i = 1, 2, \dots, 6$)
- 3: $\alpha_0 \leftarrow 1$
- 4: **for** $k = 1, 2, \dots, P$ **do**
- 5: $\mathbf{x}_k \leftarrow Q^{-1} \sum_{i=1}^6 L_i^T (\mathbf{y}_{i,k-\frac{1}{2}} - \mathbf{z}_{i,k-\frac{1}{2}})$
- 6: $\mathbf{y}_{i,k} \leftarrow \text{prox}_{\gamma_1 g_i}(L_i \mathbf{x}_k + \mathbf{z}_{i,k-\frac{1}{2}})$ ($i = 1, 2, \dots, 6$)
- 7: $\mathbf{z}_{i,k} \leftarrow \mathbf{z}_{i,k-\frac{1}{2}} + L_i \mathbf{x}_k - \mathbf{y}_{i,k}$ ($i = 1, 2, \dots, 6$)
- 8: $\alpha_k \leftarrow \frac{1 + \sqrt{1 + 4\alpha_{k-1}^2}}{2}$
- 9: $\mathbf{y}_{i,k+\frac{1}{2}} \leftarrow \mathbf{y}_{i,k} + \frac{\alpha_{k-1}-1}{\alpha_k} (\mathbf{y}_{i,k} - \mathbf{y}_{i,k-1})$ ($i = 1, 2, \dots, 6$)
- 10: $\mathbf{z}_{i,k+\frac{1}{2}} \leftarrow \mathbf{z}_{i,k} + \frac{\alpha_{k-1}-1}{\alpha_k} (\mathbf{z}_{i,k} - \mathbf{z}_{i,k-1})$ ($i = 1, 2, \dots, 6$)
- 11: **end for**
- 12: $\mathbf{z}_{i,P} \leftarrow \frac{\gamma_2}{\gamma_1} \mathbf{z}_{i,P}$ ($i = 1, 2, \dots, 6$)
- 13: **for** $k = P+1, P+2, \dots, I_{\max}$ **do**
- 14: $\mathbf{x}_k \leftarrow Q^{-1} \sum_{i=1}^6 L_i^T (\mathbf{y}_{i,k-1} - \mathbf{z}_{i,k-1})$
- 15: $\mathbf{y}_{i,k} \leftarrow \text{prox}_{\gamma_2 g_i}(L_i \mathbf{x}_k + \mathbf{z}_{i,k-1})$ ($i = 1, 2, \dots, 6$)
- 16: $\mathbf{z}_{i,k} \leftarrow \mathbf{z}_{i,k-1} + L_i \mathbf{x}_k - \mathbf{y}_{i,k}$ ($i = 1, 2, \dots, 6$)
- 17: **end for**

Output: $\mathbf{x}_l^* \leftarrow \mathbf{x}_k$

4. Numerical Simulations

To show the effectiveness of the proposed method, we conducted simulations using real PAWR data shown in Fig. 3(a). This data was acquired on March 30th, 2014, by the PAWR equipped in Suita Campus of Osaka University, Japan, and is referred as Data 1. The following simulations were executed by Matlab on iMac (OS 10.10, Intel Core i5, 2.7 GHz, 8 GB). The compressed data \mathbf{Y} was generated with compression ratio $\alpha = 0.25$, where the height parameter H_{tro} was set to 15 [km]. Each block X_l was generated by combining $s = 4$ contiguous slices. This means that the PAWR system only has to store 4 slices for sending each small block while the conventional 2D reconstruction methods⁽⁵⁾⁽⁷⁾⁽⁸⁾ have to store the entire 300 slices corresponding to one rotation of the PAWR. After sending one block, memory can be overwritten by the succeeding block. As a result, we can achieve $300/4 = 75$ times lower memory usage than those of the conventional methods⁽⁵⁾⁽⁷⁾⁽⁸⁾.

Algorithm 1 reconstructed the 3D tensors X_l from Y_l with the use of $\lambda = 4$ and $\gamma = 1.7$, and Algorithm 2 reconstructed X_l with the use of $\lambda = 4$, $\gamma_1 = 2.2$, $\gamma_2 = 1.3$ and $P = 5$. These values were set so that the reconstruction quality and the convergence rate would be the best. We compared the proposed method with the 2D methods of Mishra *et al.*⁽⁵⁾ and ours⁽⁷⁾⁽⁸⁾, which are called Conventional 1 and Conventional 2. We also compared the results of the proposed method for $s = 300$, i.e., the results of the non-blockwise reconstruction. Note that the shapes of the reconstructed blocks are different depending on the reconstruction methods, e.g., sampling and reconstruction in Conventional 1 and Conventional 2 are done slice-by-slice for each fixed elevation angle. Therefore, the measurements were not the same as those for the proposed method, but compression rate was fixed by $\alpha = 0.25$ for all methods.

We evaluated each reconstruction method by the normalized error $100 \|\mathbf{X}^* - \mathbf{X}\|_F / \|\mathbf{X}\|_F$ and the averaged computational time as shown in Table 1, where the Frobenius norm is defined by $\|\mathbf{X}\|_F := (\sum_{n_R=1}^{N_R} \sum_{n_A=1}^{N_A} \sum_{n_E=1}^{N_E} |x[n_R, n_A, n_E]|^2)^{1/2}$, and the numbers of iterations I_{\max} were set to 650, 100, 30, and 25 for Conventional 1, Conventional 2, Algorithm 1, and Algorithm 2, respectively. From Table 1, the normalized errors for Data 1 by Conventional 1 and Conventional 2 were 16.94% and 13.61%, respectively. Those by Algorithm 1 and Algorithm 2 were 9.75% and 9.78% for the entire reconstruction ($s = 300$), and were 9.88% and 9.90% for the blockwise reconstruction ($s = 4$). These results show that the proposed 3D reconstruction method outperforms the conventional 2D methods. Moreover, we can see that the deterioration due to the blockwise optimization was less than 0.5%, which is acceptable because this difference does not cause any change in the estimation of rainfall⁽⁶⁾. Although Nesterov's acceleration caused the slight deterioration of the accuracy, this is also acceptable. Therefore, the proposed 3D CS technique achieves both of low memory usage and high reconstruction accuracy. Table 2 shows the normalized errors of Algorithm 2 with different s for Data 1. From Table 2, although the reconstruction accuracy tends to become better for larger s , we judged that $s = 4$ is the best value among all factors of $N_A = 300$ in terms of both the memory usage and the reconstruction accuracy.

Figure 3 shows the reconstruction results of the 10th elevation angle. The original data \mathbf{X} and the compressed one \mathbf{Y}

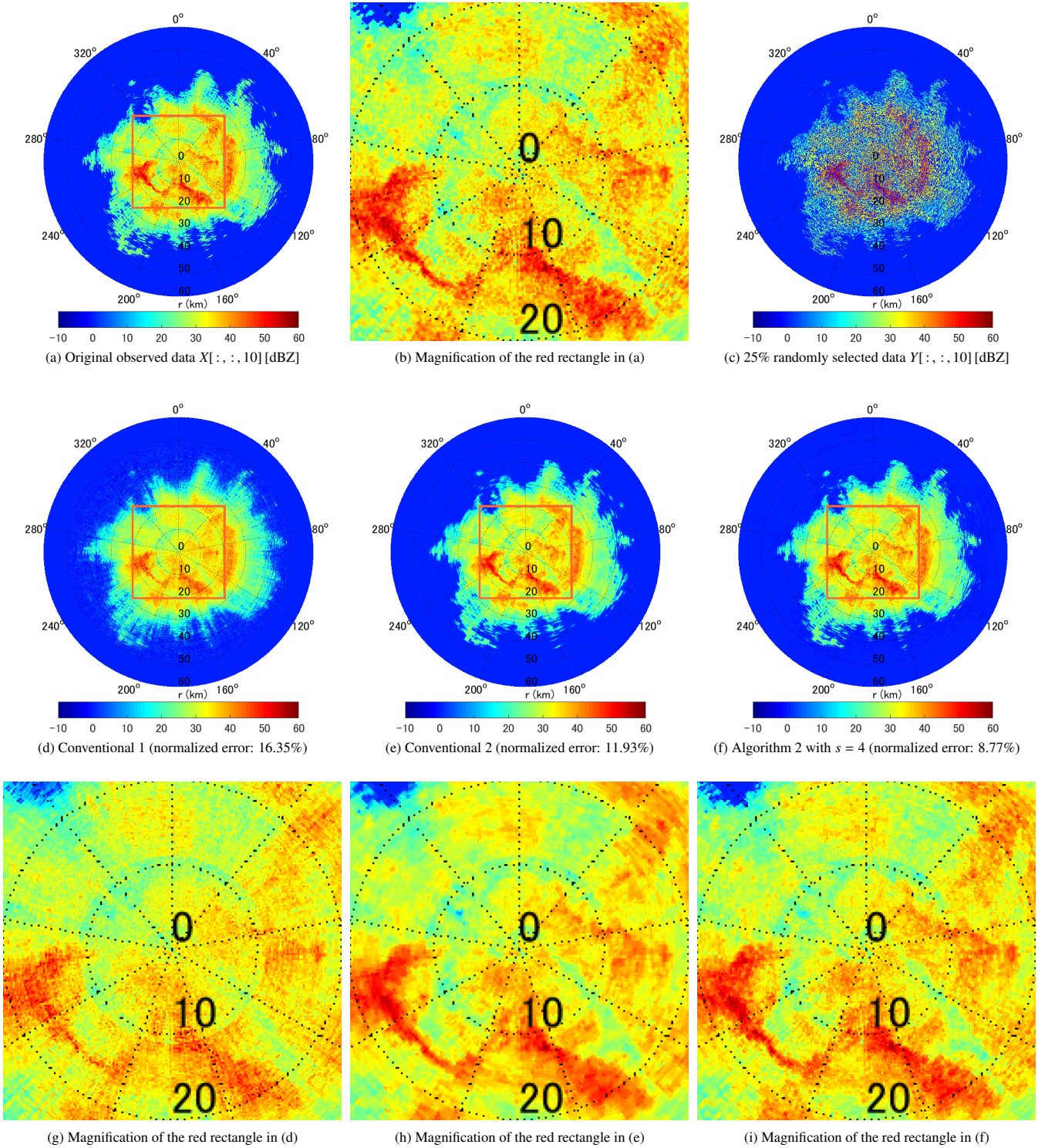


Fig. 3. Simulation results for the reflection intensity X [dBZ] observed on March 30th, 2014.

are shown in Figs. 3(a) and (c). The reconstructed one X^* by Conventional 1, Conventional 2, and Algorithm 2 with $s = 4$ are shown in Figs. 3(d), (e), and (f). Magnificated images of X and X^* are shown in Figs. 3(b), (g), (h), and (i). The normalized errors for this slice by Conventional 1 and Conventional 2 were 16.35% and 11.93%, respectively. On the other hand, that by Algorithm 2 was 8.77%. From Fig. 3, we can confirm high reconstruction quality of the proposed method.

Figure 4 shows the scatter plots of the simulation results for Data 1. Figures 4(a), (b), and (c) show the results by Con-

ventional 1, Conventional 2, and Algorithm 2 using $s = 4$, respectively. We can see that the scatter plot of the proposed method is narrower than those of the 2D methods. In particular, the plot of the proposed method more than 30dBZ seems narrower. Table 3 shows the distributions of the normalized errors in detail. Table 3 shows that the proposed 3D method outperformed the other methods for regions especially more than 30dBZ, 40dBZ and 50dBZ. These ranges indicate that it is heavily raining. Thus the proposed method may be effective for such heavy rain regions. Figure 4 also implies that the

Table 1. Normalized error and computational time of each reconstruction method.

		Conventional 1	Conventional 2	Algorithm 1 ($s = 300$)	Algorithm 2 ($s = 300$)	Algorithm 1 ($s = 4$)	Algorithm 2 ($s = 4$)
Normalized Error [%]	Data 1 (2014/3/30)	16.94	13.61	9.75	9.78	9.88	9.90
	Data 2 (2014/1/8)	20.51	17.21	12.49	12.48	12.69	12.65
	Data 3 (2013/6/19)	16.65	13.37	9.56	9.62	9.68	9.72
	Data 4 (2013/5/10)	30.35	21.03	15.15	15.33	15.61	15.82
Averaged Computational Time [sec]		2,180	678	304	223	314	242
(Computational Time per Slice or Block)		(19.82 per Slice)	(6.16 per Slice)	—	—	(4.19 per Block)	(3.23 per Block)

Table 2. Normalized errors depending on s for Data 1.

s	2	3	4	5	6	10	20	30	60	100	150
Error	9.99	9.93	9.90	9.90	9.91	9.87	9.85	9.83	9.81	9.82	9.80

Table 3. Normalized error distributions for Data 1.

	Conventional 1	Conventional 2	Algorithm 2 ($s = 4$)
Normalized Error [%]	16.94	13.61	9.90
≥ 20 dBZ	12.93	9.38	6.75
≥ 30 dBZ	11.00	7.42	5.32
≥ 40 dBZ	12.77	7.68	5.06
≥ 50 dBZ	16.88	8.03	4.93

true PAWR data do not take the reflection intensities less than 15dBZ. This is because 15dBZ is too small to be valid measurements, and hence the system is designed to discard such values. The proposed method does not use this knowledge, and if do, the reconstruction quality can be further improved.

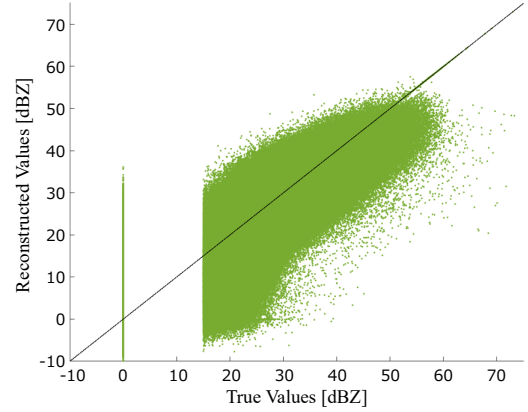
Table 1 also shows the computational time of each method. From Table 1, we find that both Algorithms 1 and 2 achieved better reconstruction accuracy with less computational time than Conventional 1 and Conventional 2. In addition, Algorithm 2 is approximately 1.3 times faster than Algorithm 1, and hence Nesterov's technique is effective for acceleration.

We further conducted simulations for other data acquired on January 8th, 2014, June 19th, 2013, and May 10th, 2013, which are referred as Data 2, Data 3, and Data 4, respectively. The normalized errors for each data are shown in Table 1 in the same manner as Data 1. Further, Figs. 5, 6, and 7 show the reconstruction results of the 10th elevation angle for Data 2, Data 3, and Data 4, respectively. From Table 1 and these figures, we can see that the proposed method robustly achieves better reconstruction results than the conventional methods.

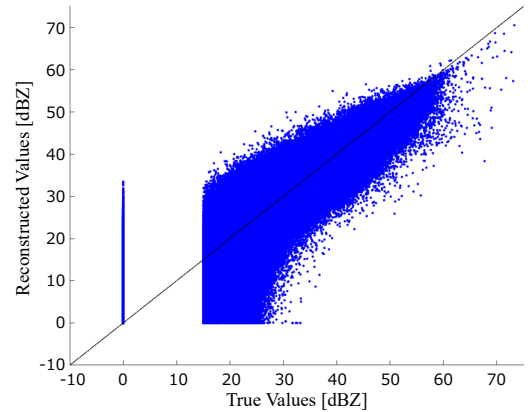
In the above simulations, the number of the blocks X_l is 75. Yet, to complete the reconstruction for all thirteen parameters of the PAWR, the proposed method requires $3.23 \times 75 \times 13 \approx 3,150$ seconds. Since the reconstruction should be completed within 30 seconds, 105 times acceleration is required approximately. To further accelerate Algorithm 2, implementation by some compiler language like C is effective. In addition, since the reconstruction for each block can be performed in a parallel way, the computation based on GPU is also effective. If each block can be reconstructed by a separate computer in parallel, $105/75 \approx 1.4$ times acceleration is required to transfer all parameters observed by the PAWR data in real time.

5. Conclusion

This paper proposed a fast high-quality 3D CS technique for transferring the PAWR data in a public internet line. First, we summarized our compression and reconstruction schemes based on random sampling in the troposphere and blockwise convex optimization, respectively. In the reconstruction part, we defined a new cost function that expresses a prior knowl-



(a) Conventional 1



(b) Conventional 2

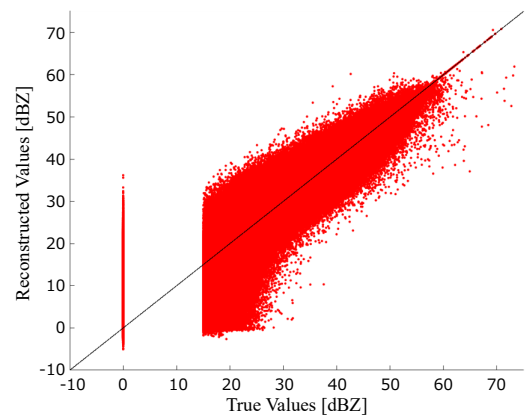
(c) Algorithm 2 with $s = 4$

Fig. 4. Scatter plot of each method for Data 1.

edge such as the local similarity and sparsity of the 3D PAWR data in the spatial and frequency domains. Because the cost

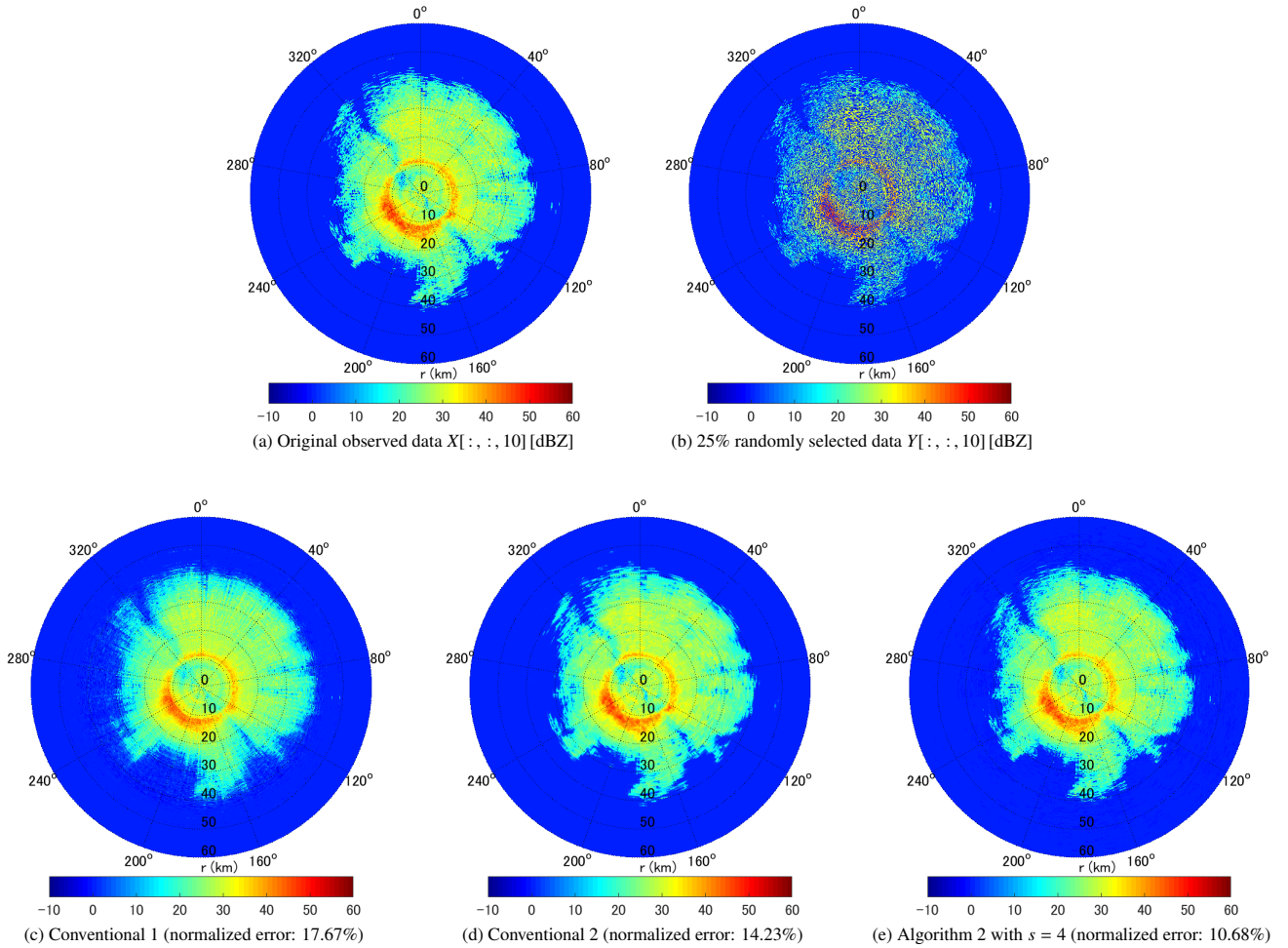


Fig. 5. Simulation results for the reflection intensity X [dBZ] observed on January 8th, 2014.

function is convex, an efficient reconstruction algorithm was derived by SDMM. Then, for improvement of the computational speed, we applied Nesterov's acceleration technique to SDMM. Numerical experiments using real data showed that the proposed method achieves low memory usage, high accuracy, and fast reconstruction compared with 2D methods. Since the reconstruction can be performed for each block in a parallel way, our method can be further accelerated by GPU.

Acknowledgments

This work was supported by JSPS KAKENHI Grant Number 17H02069. The authors are grateful to Prof. Takashi Ijiri in Shibaura Institute of Technology for fruitful discussions.

References

- (1) Committee on Extreme Weather Events and Climate Change Attribution: Attribution of Extreme Weather Events in the Context of Climate Change, Washington D.C.: The National Academy Press (2016)
- (2) F. Mizutani, M. Wada, T. Ushio, E. Yoshikawa, S. Satoh, and T. Iguchi: "Development of active phased array weather radar", in Proc. 35th Conf. Radar Meteor., Pittsburgh, PA: 4 pages (2011)
- (3) E. Yoshikawa, T. Ushio, Z. Kawasaki, S. Yoshida, T. Morimoto, F. Mizutani, and M. Wada: "MMSE beam forming on fast-scanning phased array weather radar", IEEE Trans. Geosci. Remote Sens., Vol.51, No.5, pp.3077-3088 (2013)
- (4) F. Mizutani, T. Ushio, E. Yoshikawa, S. Shimamura, H. Kikuchi, M. Wada, S. Satoh, and T. Iguchi: "Fast-scanning phased-array weather radar with angular imaging technique", IEEE Trans. Geosci. Remote Sens., Vol.56, No.5, pp.2664-2673 (2018)
- (5) K. V. Mishra, A. Kruger, and W. F. Krajewski: "Compressed sensing applied to weather radar", in Proc. IEEE Int. Geosci. Remote Sens. Symp., Quebec City, QC, Canada: pp.1832-1835 (2014)
- (6) S. Shimamura, H. Kikuchi, T. Matsuda, G. Kim, E. Yoshikawa, Y. Nakamura, and T. Ushio: "Large-volume data compression using compressed sensing for meteorological radar", Electron. Comm. Jpn., Vol.99, No.10, pp.103-111 (2016)
- (7) R. Kawami, A. Hirabayashi, N. Tanaka, M. Shibata, T. Ijiri, S. Shimamura, H. Kikuchi, G. Kim, and T. Ushio: "2-dimensional high-quality reconstruction of compressive measurements of phased array weather radar", in Proc. Asia-Pac. Signal Inf. Process. Assoc. Annual Summit Conf. (APSIPA ASC), Jeju, South Korea: 7 pages (2016)
- (8) R. Kawami, A. Hirabayashi, N. Tanaka, M. Shibata, T. Ijiri, S. Shimamura, H. Kikuchi, G. Kim, and T. Ushio: "Simple compression technique for phased array weather radar and 2-dimensional high-quality reconstruction", IEEE Trans. Electron. Inf. Syst., Vol.137, No.7, pp.864-870 (2017)
- (9) R. Kawami, H. Kataoka, D. Kitahara, A. Hirabayashi, T. Ijiri, S. Shimamura, H. Kikuchi, and T. Ushio, "Fast high-quality three-dimensional reconstruction from compressive observation of phased array weather radar," in Proc. Asia-Pac. Signal Inf. Process. Assoc. Annual Summit Conf. (APSIPA ASC), Kuala Lumpur, Malaysia: pp.44-49 (2017).
- (10) E. Kuddeki and F. Stürücü, "Radar interferometric imaging of field-aligned plasma irregularities in the equatorial electrojet," *Geophys. Res. Lett.*, Vol.18, No.1, pp.41-44 (1991)
- (11) E. Yoshikawa, T. Ushio, Z. Kawasaki, S. Yoshida, T. Morimoto, F. Mizutani, and M. Wada: "MMSE Beam Forming on Fast-Scanning Phased Array Weather Radar," IEEE Trans. Geosci. Remote Sens., Vol. 51, No. 5, pp.3077-3088 (2013)
- (12) D. Kitahara, M. Nakahara, A. Hirabayashi, E. Yoshikawa, H. Kikuchi, and T. Ushio, "Nonlinear beamforming via convex optimization for phased array weather radar," in Proc. Asia-Pac. Signal Inf. Process. Assoc. Annual Summit Conf. (APSIPA ASC), Honolulu, HI: pp.1831-1835 (2018)

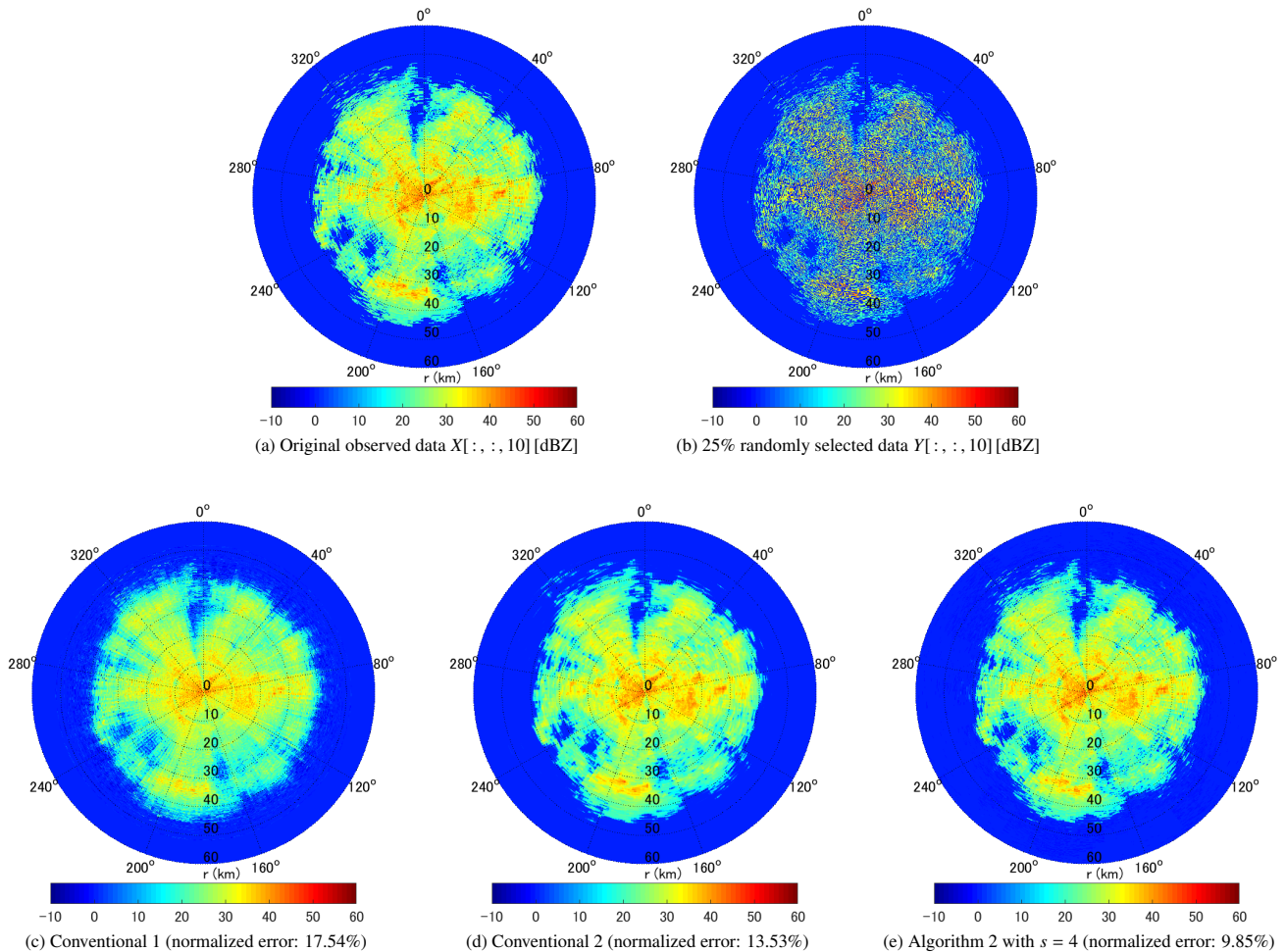


Fig. 6. Simulation results for the reflection intensity X [dBZ] observed on June 19th, 2013.

- (13) D.L. Donoho: "Compressed sensing", *IEEE Trans. Inf. Theory*, Vol.52, No.4, pp.1289-1306 (2006)
- (14) E.J. Candès and M.B. Wakin: "An introduction to compressive sampling", *IEEE Signal Process. Mag.*, Vol.25, No.2, pp.21-30 (2008)
- (15) Y.C. Eldar and G. Kutyniok, Eds.: *Compressed Sensing: Theory and Applications*, Cambridge, MA: Cambridge University Press (2012)
- (16) R. Baraniuk and P. Steeghs: "Compressive radar imaging", in *Proc. IEEE Radar Conf.*, Boston, MA: pp.128-133 (2007)
- (17) M.A. Herman and T. Astronomer: "High-resolution radar via compressed sensing", *IEEE Trans. Signal Process.*, Vol.57, No.6, pp.2275-2284 (2009)
- (18) J.H.G. Ender: "On compressive sensing applied to radar", *Signal Process.*, Vol.90, No.5, pp.1402-1414 (2010)
- (19) P. Meischner, Ed.: *Weather Radar: Principles and Advanced Applications*, New York, NY: Springer (2004)
- (20) T.Y. Yu, L. Ding, and S. Ozturk: "Application of compressive sensing to refractivity retrieval with a network of radars", in *Proc. IEEE Radar Conf.*, Kansas City, MO: pp.757-761 (2011)
- (21) D. Gabay and B. Mercier: "A dual algorithm for the solution of nonlinear variational problems via finite element approximation", *Comput. Math. Appl.*, Vol.2, No.1, pp.17-40 (1976)
- (22) P.L. Combettes and J.C. Pesquet, Eds.: *Fixed-Point Algorithms for Inverse Problems in Science and Engineering*, New York, NY: Springer (2011)
- (23) L. Condat: "A generic proximal algorithm for convex optimization—Application to total variation minimization", *IEEE Signal Process. Lett.*, Vol.21, No.8, pp.985-989 (2014)
- (24) Y.E. Nesterov: "A method for solving the the convex programming problem with convergence rate $O(1/k^2)$ ", *Sov. Math. Dokl.*, Vol.27, No.2, pp.372-376 (1983)
- (25) A. Beck and M. Teboulle: "A fast iterative shrinkage-thresholding algorithm for linear inverse problems", *SIAM J. Imag. Sci.*, Vol.2, No.1, pp.182-202 (2009)
- (26) T. Goldstein, B. O'Donoghue, S. Setzer, and R. Baraniuk: "Fast alternating direction optimization methods", *SIAM J. Imag. Sci.*, Vol.7, No.3, pp.1588-1623 (2014)
- (27) M. Yamagishi, D. Kitahara, and I. Yamada: "A fast dual iterative algorithm for convexly constrained spline smoothing", in *Proc. IEEE Int. Conf. Acoust. Speech Signal Process. (ICASSP)*, Shanghai, China: pp.4538-4542 (2016)

Ryosuke Kawami (Student Member) received the B.E. and M.E. degrees in computer science from Ritsumeikan University, Shiga, Japan, in 2017 and 2019, respectively. His research interests include compressed sensing and its applications. He received the Young Researcher Paper Award of IEEJ Transactions on Electronics, Information and Systems in 2018.



Daichi Kitahara (Non-member) received the B.E. degree in computer science in 2012, and the M.E. and Ph.D. degrees in communications and computer engineering in 2014 and 2017 from the Tokyo Institute of Technology, Tokyo, Japan, respectively. From 2014 to 2017, he was a recipient of the Research Fellowship of the Japan Society for the Promotion of Science (JSPS). Since 2017, he has been an Assistant Professor with the College of Information Science and Engineering, Ritsumeikan University, Shiga, Japan. His current research interests are in signal processing and its applications, inverse problem, optimization theory, and multivariate spline theory.



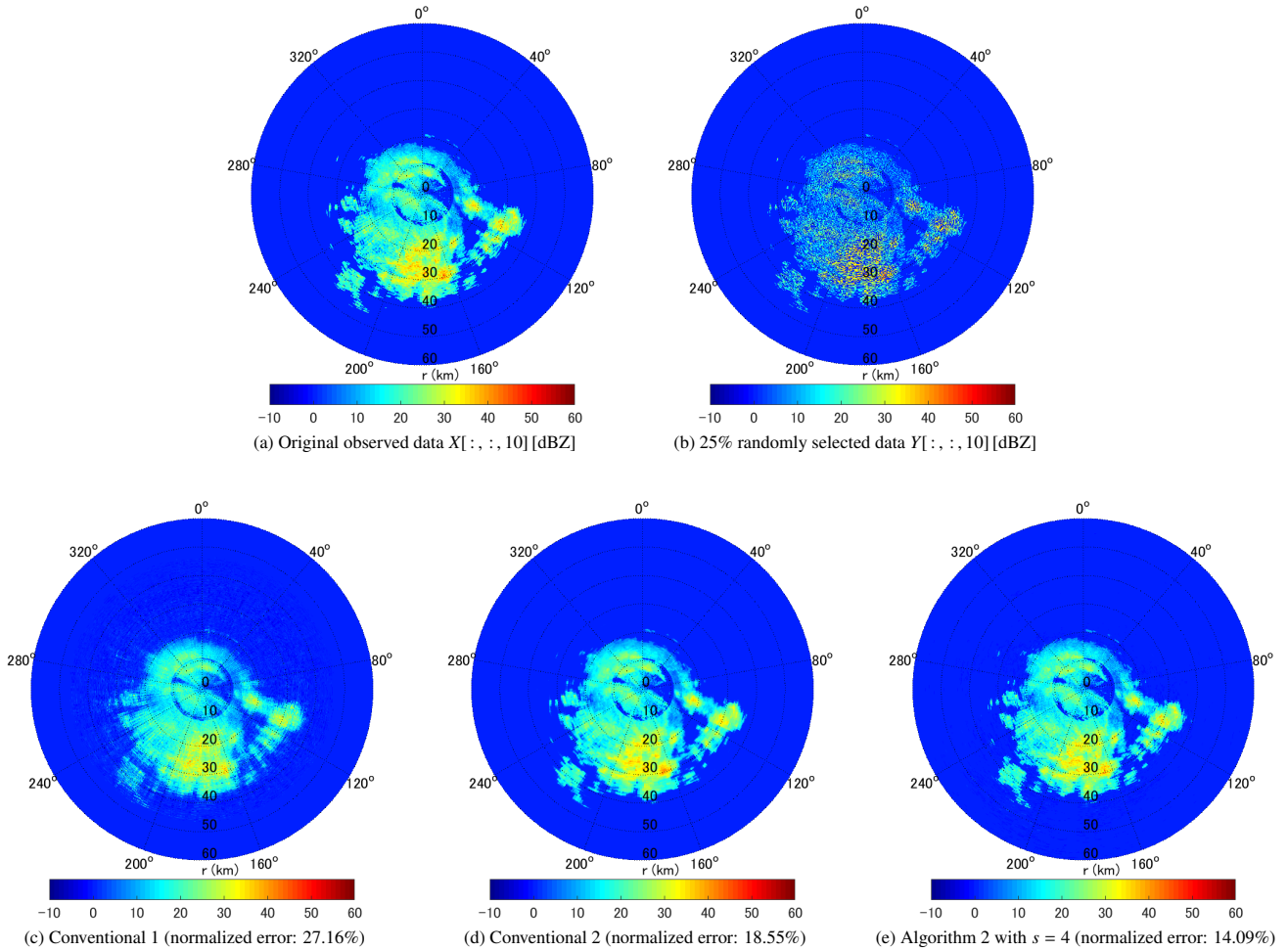


Fig. 7. Simulation results for the reflection intensity X [dBZ] observed on May 10th, 2013.

Akira Hirabayashi (Non-member) received his D.E. degree in computer science in 1999, from the Tokyo Institute of Technology, Tokyo, Japan. Currently, he is a Professor of the College of Information Science and Engineering, Ritsumeikan University, Shiga, Japan. His research interests include compressed sensing, sampling theory, and signal and image processing. Prof. Hirabayashi is also a member of the Institute of Electrical and Electronics Engineers (IEEE) and the Acoustical Society of Japan (ASJ).



Hiroshi Kikuchi (Member) received the B.S. degree from the Department of Engineering, Doshisha University, Kyoto, Japan, in 2008, and the M.S. and Ph.D. degrees from the Division of Electrical, Electronic, and Information Engineering, Osaka University, Suita, Japan, in 2010 and 2013, respectively. He joined the Division of Electrical, Electronic, and Information Engineering, Osaka University as a Specially Appointed Researcher in 2013. In 2017, he was a Research Assistant Professor at Tokyo Metropolitan University. In 2018, he joined The University of Electro-Communications, where he is currently an Assistant Professor. His research specialties are the remote sensing for an atmospheric electricity with space-borne platforms, the weather radar remote sensing, and a development of the radar system.



Eiichi Yoshikawa (Non-member) received the B.E. degree in aerospace engineering from Osaka Prefecture University, Sakai, Japan, in 2005, and the M.E. and Ph.D. degrees from Osaka University, Suita, Japan, in 2008 and 2011, respectively. In 2011, he was a Post-Doctoral Researcher with Osaka University and Colorado State University, Fort Collins, CO, USA, and also a Post-Doctoral Fellow of the Research Fellowship for Young Scientists sponsored by the Japan Society for the Promotion of Science. In 2012, he joined



the Japan Aerospace Exploration Agency (JAXA), Mitaka, Japan, where he is currently an Associate Senior Researcher. He is a Visiting Associate Professor with Tokyo Metropolitan University, Tokyo, Japan. His research interests include weather radar remote sensing, radar-based analyses, and applications for general and aviation weather.

Tomoo Ushio (Senior Member) received the B.S., M.S., and Ph.D. degrees in electrical engineering from Osaka University, Suita, Japan, in 1993, 1995, and 1998, respectively. He was with the Global Hydrology and Climate Center, Huntsville, AL, USA, as a Post-Doctoral Researcher from 1998 to 2000. In 2000, he joined the Department of Aerospace Engineering, Osaka Prefecture University, Sakai, Japan, as an Assistant Professor. In 2006, he joined the Division of Electrical, Electronic and Information Engineering, Osaka University, as an Associate Professor. In 2017, he joined the Department of Aeronautics and Astronautics, Tokyo Metropolitan University, as a Professor. Since 2019, he has been a Professor in Osaka University. His research specialties are radar-based remote sensing, passive and active remote sensing of atmosphere from space-borne platforms, and atmospheric electricity.

